Linearisation of a ship propulsion system model

Stapersma, Douwe; Vrijdag, Arthur

DOI
10.1016/j.oceaneng.2017.07.014

Publication date
2017

Document Version
Accepted author manuscript

Published in
Ocean Engineering

Citation (APA)
Stapersma, D., & Vrijdag, A. (2017). Linearisation of a ship propulsion system model. *Ocean Engineering*, *142*, 441-457. https://doi.org/10.1016/j.oceaneng.2017.07.014

Link to formal publication Ocean Engineering (Elsevier): https://doi.org/10.1016/j.oceaneng.2017.07.014

Linearisation of a Ship Propulsion System Model

D. Stapersma[a,1], A. Vrijdag[a,2,*]

[a] *Delft University of Technology, Faculty of Mechanical, Maritime and Materials Engineering, Mekelweg 2, 2628CD, Delft, the Netherlands*

Abstract

The understanding, modelling and analysis of the behaviour of a non-linear ship propulsion plant are of great importance for conceptual system design, component selection, selection of control strategy and for propulsion control system tuning. Conceptual propulsion system design activities, such as deciding the combinator curve, require a relatively simple steady state simulation model, while propulsion controller design and tuning requires a non-linear time domain simulation model which captures the intricacies of the propulsion plant. In this paper a linearised model of the uncontrolled ship propulsion system is derived which can be used for analysis of propulsion system behaviour in waves and for initial controller design and tuning. Furthermore a thorough analysis is made of the conditions under which local instability of the system can occur. In a follow up paper the linearised model is extended and verified by means of comparison with a non-linear model. There it is furthermore used to investigate the effect of engine governor settings on a propulsion plant when sailing in waves at different encounter frequencies. The authors believe that, due to its transparency and clear link to well known parameters and variables, the linearised core propulsion system model as derived in this paper should appeal to marine system engineers, control engineers and hydrodynamicists alike. The linearised model should however not be seen as the replacement for a non-linear model, but rather as an additional tool that can be used.

Keywords: Ship Propulsion System, Propulsion System Dynamics, Propulsion System Stability, Linear Ship Propulsion Model

1. Introduction

The use of linearised models is common practise in many fields of engineering because they have some favourable properties over non-linear models. Linear models are often more simple and require less parameter and system knowledge compared to non-linear models, although this advantage reduces as soon as linear models are to be generated for multiple operating regions. The main reason to derive a linear model in this paper is that linear models can be used to predict system behaviour in the frequency domain. Linearisation does however come at a price: a linearised model is only valid in the neighbourhood of equilibrium (Franklin et al. (1986)). The size of the region in which a linearised model is valid can be small or can be large, but should remain a point of attention while using such a model. This is the reason why the linearised ship propulsion model should not be seen as the replacement for a non-linear model, but rather as an additional tool that can be used. In this paper the behaviour of the ship propulsion system in the frequency domain is investigated by derivation and analysis of the transfer functions. The transparent derivation of the linearised system reveals the main parameters and variables that govern the dynamic performance of the core ship propulsion system. These main parameters and variables are shown to be four derivatives in the open water propeller diagram and one derivative of the ship resistance curve. Inertia of the propulsion system is introduced by two (operating point dependent) time constants which among other variables respectively include the polar moment of inertia of the rotating shaft system and the mass of the ship. These seven parameters are well known to marine system engineers who use their respective values for all sorts of calculations, ranging from torsional shaft vibration analysis to the calculation of maximum ship speed.

There are various examples where engineers and scientists coming from all sorts of disciplines have attempted to get a grip on ship propulsion system dynamics and behaviour in the frequency domain. Two examples of a theoretical approach coming from a control perspective are reported by van Spronsen and Tousain (2001) and Xiros (2004), where in both cases a linearised model is used to apply H_∞ controller techniques aiming at prevention of diesel engine overloading. Although the work is highly valuable, the drawback is that the used plant models are not directly related to the commonly used parameters and therefore have less appeal to marine system engineers and hydrodynamicists. An example coming from a hydrodynamic perspective, involving research into dynamic behaviour of

*Corresponding author. Delft University of Technology, Faculty of Mechanical, Maritime and Materials Engineering, Mekelweg 2, 2628CD, Delft, the Netherlands

Email address: a.vrijdag@tudelft.nl (A. Vrijdag)

[1] Retired Professor of Marine Engineering

[2] Assistant Professor

propellers in waves is given in van Terwisga et al. (2004). In that case it was concluded that the propulsion control system and its parameters plays an important role in the behaviour of the propeller in waves. The analysis of the effect of the propulsion control system settings on the prime mover was however strongly simplified. An early example of linearization is given by Clarke (1980). He includes ship inertia but ignores shaft speed dynamics and implicitly controls either shaft speed or engine power or engine torque or even ship speed, but all for fixed pitch propeller. Added resistance due to manoevring is taken into account but disturbances of wake speed are not. He does not normalize his equations and the derivation in general lacks clarity. Another example related to the linearisation of the ship propulsion plant is reported by Blanke (1981) and repeated in Fossen (1994). There a linearised model was derived from a manoeuvring/motion control point of view. This model has many of the features that will be used in the present paper as well, i.e. the dynamics of ship and shaft speed, engine torque as the input of the linearized model, added ship resistance as a result of sway and disturbance of wake speed caused by waves. The model is restricted to fixed pitch propellers. Also the coefficients that were used to describe the propeller performance were only implicitly related to derivatives in the open water propeller diagram. The linearized model and in particular the main differential equations are not normalized which makes the derivation from the linearised model equations to the the final transfer functions unnecessary complicated and not transparent and therefore made it hard for others to use the model. Also the linearized model is not fully linear as some products of perturbations are still present. A notable effort to linearise a gas turbine driven ship propulsion system is reported by Kidd et al. (1985). The work there is similar to the work reported in this paper, in the sense that it is an attempt to derive linear relationships between inputs and outputs. However, the derivation there does not take into account the system inputs related to ship resistance and propeller wakefield disturbances. The most important shortcoming is however the non-transparent linearised propeller model, which does not match the generally available propeller data from open water diagrams. Finally a simulation model is described but no results are shown, which makes it hard to assess the model.

It may be concluded that linearized models were developed in the eighties of the last century but for several reasons did not appeal to the maritime industry and seem not to be used frequently anymore. This paper intents to revive linear models and indicate when and where they could have some use. The authors believe that, due to its transparency and clear link to well known parameters and variables, the linearised propulsion system model as derived in this paper should appeal to marine system engineers, control engineers and hydrodynamicists alike. Its transparency allows for modular expansion of which an example is already given by Shi (2013) where an early version of the theory as reported in this paper is used to analyse the dynamic performance of a trailing suction hopper dredger. Moreover, the linearised model of the propulsion system was extended with a linearised model of the dredging system including engine driven dredging pump and suction pipe. Other extensions related to drag head resistance and non-symmetric propeller load between the shaft lines were also made.

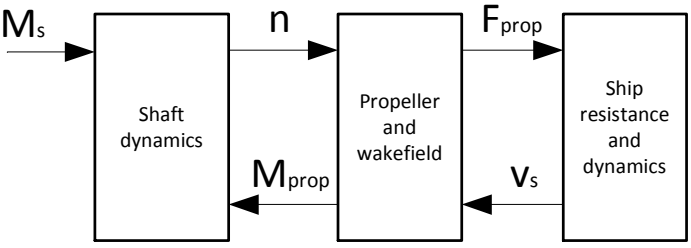

Figure 1: General core ship propulsion block diagram.

This paper is structured as follows: In the first part the linearised core model is reported and Bode plots of the system are discussed. In the second part of the paper the stability of the system is analysed and particular cases under which the system might become locally unstable are investigated. Finally conclusions are drawn and recommendations for further research are given. For transparency the main derivations are included in the appendices.

2. General ship propulsion block diagram

Fig. 1 shows a general ship propulsion block diagram. It contains the (non-linear) dynamics of a ship propulsion plant, excluding the propulsion machine and the propulsion control system. On the right hand side the ship translation dynamics are included, based on a force balance between propeller thrust and ship resistance. When those two forces are out of balance, a net force will result in a change of momentum via:

$$\frac{d(m_{ship} \cdot v_s)}{dt} = F_{prop} - F_{ship} \tag{1}$$

in which m_{ship} is the total ship mass including added water mass. The exact definition of F_{prop} and F_{ship} including their relation with propeller thrust T and ship resistance R are given later. On the left hand side the shaft rotation dynamics are included, dealing with the balance between propeller and shaft torque. In the same way as in the translation dynamics a net torque will cause a change of angular momentum via:

$$2\pi \frac{d(I_p \cdot n)}{dt} = M_s - M_{prop} \tag{2}$$

in which I_p is the total polar moment of inertia of the rotating shaft system including propeller and entrained water. Note that for clarity no gearbox is included in the block diagram. Further note that for now no choice is made with

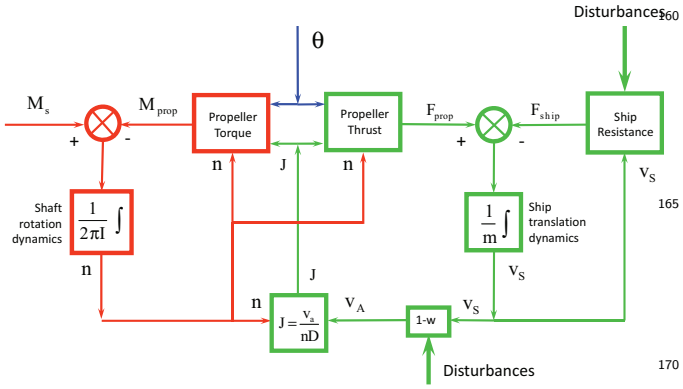

Figure 2: Detailed core ship propulsion block diagram.

regard to the type of propulsion machine: the choice for a diesel engine, gas turbine, electric motor or any other device in principle is open. This selection is made in a follow up paper which deals with the extension and application of the core linearised propulsion systems model.

In the middle of the block diagram the propeller thrust and torque are modelled based on the open water diagram of the propeller under consideration:

$$\begin{aligned} T &= \rho \cdot n^2 \cdot D^4 \cdot K_T(J,\theta) \\ Q &= \rho \cdot n^2 \cdot D^5 \cdot K_Q(J,\theta) \\ J &= \frac{v_a}{n \cdot D} \end{aligned} \tag{3}$$

The instantaneous values of thrust coefficient K_T and torque coefficient K_Q as a function of advance ratio J and propeller pitch θ are based on lookup tables of the open water diagram of the propeller(s) under consideration. Note that this approach inherently neglects any hydrodynamic propeller dynamics. The relation between T and F_{prop} and between Q and M_{prop} and between v_a and v_s is given later.

The core propulsion system as shown in Fig. 1 is linearised in the following sections. However, before this is done, a more detailed overview of the system is given in Fig. 2. This block diagram, as modified from Stapersma (2000) shows the ship and shaft dynamics under the assumption of constant ship mass and constant shaft inertia as well as Eq. (3). Besides the two input variables propeller pitch θ and shaft torque M_s it shows two disturbance inputs acting on the ship resistance and on the wakefield. Resistance disturbances can for instance be caused by wind, waves, shallow water, or changes in ship draft or trim and act on the ship speed loop. Wakefield disturbances can be caused by for instance ship motions, orbital wave velocities in the propeller plane or manoeuvres and act directly on the shaft speed loop, and indirectly on the ship speed loop.

3. Linearisation

The ship propulsion system shown in Fig. 2 is non-linear. The non-linearities can be classified into 3 categories:

1. Non-linearity due to curvature in the characteristics of component models. Clear examples are the curvature of the K_T and K_Q lines in the propeller open water diagram as well as the non-linearity in the P/D-direction.
2. Non-linearity due to multiplicative action in the mathematical model of the system. This includes multiplication (e.g. $T = \rho \cdot n^2 \cdot D^4 \cdot K_T(J,\theta)$), division (e.g. $J = \frac{v_a}{nD}$) and general power operations (e.g. $R = \alpha \cdot v_s^e$).
3. Non-linearity due to a hard limit in the model. Examples are: saturation of actuators (mechanical end-stop of a fuel rack, or minimum and maximum pitch of a hydraulic CPP system) or limits due to protective features in the engine governor.

The goal of this section is to find a linear representation of the core propulsion system, so that the frequency domain behaviour of a ship propulsion plant can be determined. The effect of neglecting the mentioned three types of non-linearities is investigated in the follow up paper, in which a comparison of system behaviour is made with a non-linear model. In particular the fact that non-linearities of the third category are completely neglected by a linearised model, is an important limitation. The linearisation of the uncontrolled core system has been done by Stapersma (2016), and the notation as well as the basic derivation are given in Appendix B and Appendix C. A summary of the results from those appendices is given below.

3.1. Normalisation and Linearisation

As shown in Appendix B, a variable that is the product of powers of other variables:

$$Z = c \cdot Y^e \cdot X \tag{4}$$

can be linearised and normalised. By using the shorthand notation for differential increment as given by:

$$\delta Z^* \equiv \frac{\delta Z}{Z_0}, \delta Y^* \equiv \frac{\delta Y}{Y_0}, \delta X^* \equiv \frac{\delta X}{X_0} \tag{5}$$

Eq. (4) can be approximated by:

$$\delta Z^* = \delta X^* + e \cdot \delta Y^* \tag{6}$$

The latter equation relates the relative change in output Z to the relative change in inputs X and Y, where the constant e, which was present as an exponent in the original Eq. (4) has changed to a constant multiplication factor. Secondly the multiplication of X and Y has turned into a summation.

Under the assumption of constant m_{ship} and I_p, Eqs. (1) and (2) can be written as:

$$2\pi \cdot I_p \cdot \frac{dn}{dt} = M_s - M_{prop} \tag{7}$$

and

$$m_{ship} \cdot \frac{dv_s}{dt} = F_{prop} - F_{ship} \tag{8}$$

As derived in Appendix C, the normalised and linearised version of Eq. (7) is:

$$\tau_n \frac{dn^*}{dt} = \delta M_b^* - (2-b)\delta n^* - b\delta v_s^* + b\delta w^* - q\delta\theta^* \tag{9}$$

which gives the relation between shaft acceleration, the two state variables δn^* and δv_s^* and the inputs brake engine torque δM_b^*, wake disturbance δw^* and propeller pitch $\delta\theta^*$. Likewise the normalised and linearised version of Eq. (8) is:

$$\tau_v \frac{dv_s^*}{dt} = (2-a)\delta n^* - (e-a)\delta v_s^* - \delta\alpha^* - a\delta w^* + p\delta\theta^* \tag{10}$$

which gives the relation between ship acceleration, the two system states and resistance disturbance $\delta\alpha^*$, wake disturbance δw^* and propeller pitch $\delta\theta^*$.

In these two equations 7 parameters are used. The normalised propeller derivatives a, b, p and q are defined as:

$$a \equiv \frac{J_0}{K_{T,0}} \cdot \left.\frac{\delta K_T}{\delta J}\right|_\theta, \quad p \equiv \frac{\theta_0}{K_{T,0}} \cdot \left.\frac{\delta K_T}{\delta \theta}\right|_J \tag{11}$$

$$b \equiv \frac{J_0}{K_{Q,0}} \cdot \left.\frac{\delta K_Q}{\delta J}\right|_\theta, \quad q \equiv \frac{\theta_0}{K_{Q,0}} \cdot \left.\frac{\delta K_Q}{\delta \theta}\right|_J \tag{12}$$

Furthermore the 2 integration constants τ_n and τ_v are defined as:

$$\tau_n \equiv \frac{2\pi \cdot I_p \cdot n_0}{M_{s,0}}, \quad \tau_v \equiv \frac{m_{ship} \cdot v_{s,0}}{F_{ship,0}} \tag{13}$$

Finally the normalised resistance curve steepness e is defined as:

$$e \equiv \frac{v_{s,0}}{R_0} \cdot \left.\frac{\delta R}{\delta v_s}\right|_\alpha \tag{14}$$

Contour plots of a, b, p and q for a particular propeller are shown in Figs. 3, 4, 5 and 6. Note that the actual $J - K_T - K_Q$ relations for multiple pitch values are not shown to avoid confusion. Further note that alternatively to the $J - K_T - K_Q$ approach as shown here, the linearisation of the propeller performance can also be modelled via the four quadrant $\beta - C_T^* - C_Q^*$ approach, which is elaborated in Appendix D.

An example of the normalised steepness parameter e is shown in Fig. 7. Note that the humps and hollows in the resistance curve are magnified when plotted in this way.

The block diagram shown in Fig. 8, which is equivalent with Fig. C.11, is the visual representation of Eqs. (9) and (10). Note that this presentation, aside from a weak coupling via the returning b path, shows two first order systems in series. This aligns with the fact that, in case of a water jet driven system, b is close to zero and the shaft system behaviour is almost uncoupled from the ship speed.

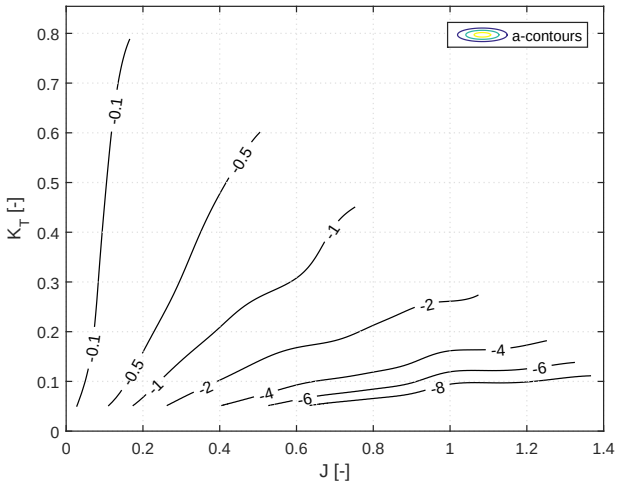

Figure 3: Contour plot of propeller derivative a.

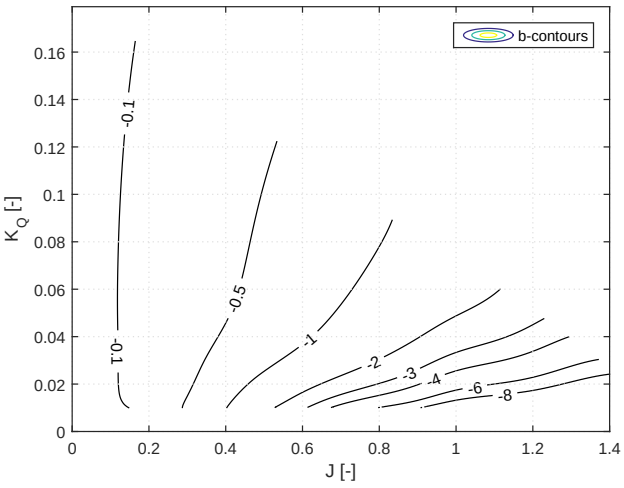

Figure 4: Contour plot of propeller derivative b.

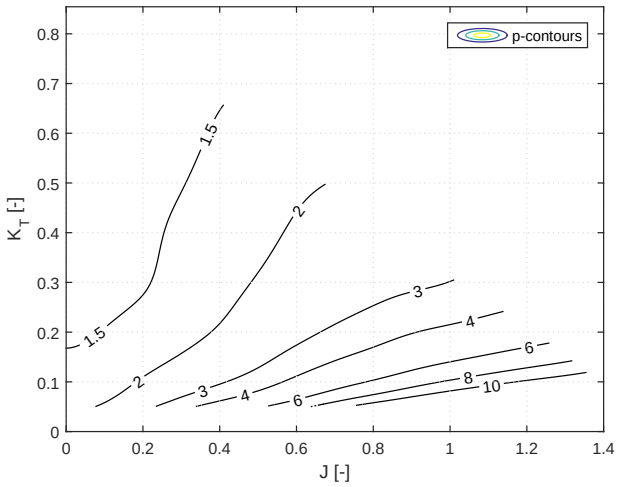

Figure 5: Contour plot of propeller derivative p.

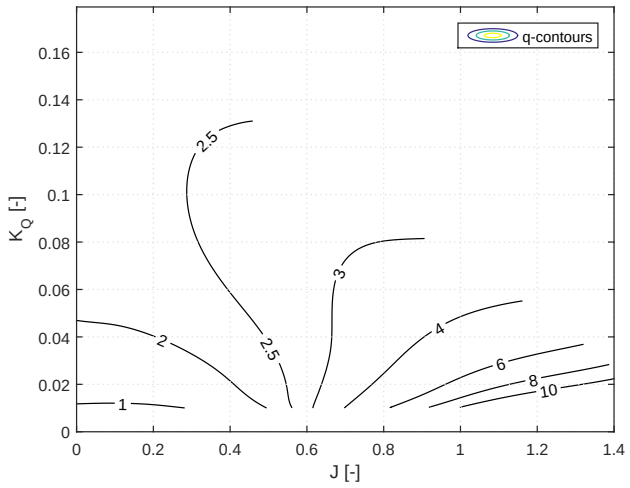

Figure 6: Contour plot of propeller derivative q.

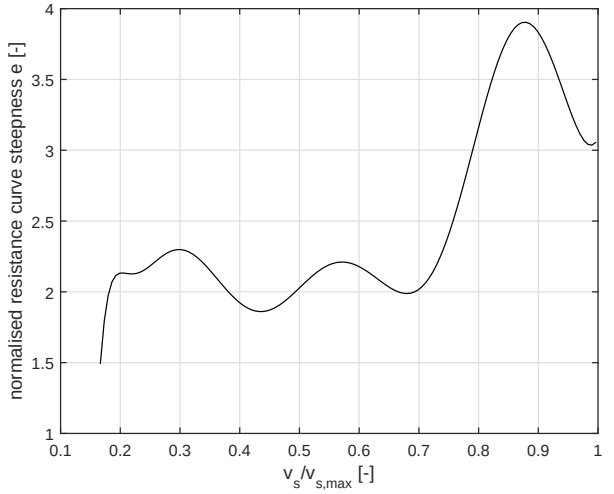

Figure 7: Normalised ship resistance curve steepness.

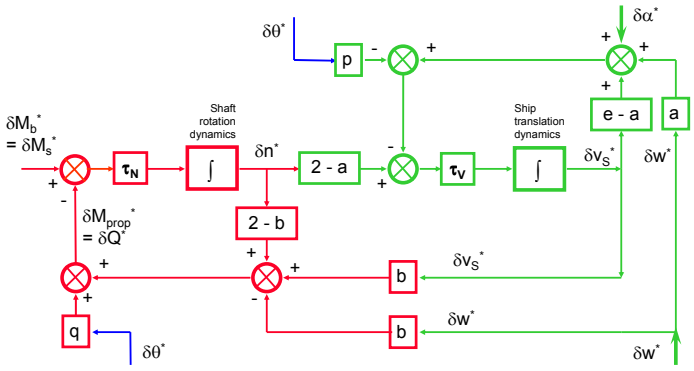

Figure 8: Linearised block diagram of the core propulsion system.

4. Laplace Transfer Functions

The derivation of the transfer functions of the system described by Eqs. (9) and (10) is given in Appendix E. The transfer functions from the 4 inputs to the state variable δn^* are given by:

$$\frac{\delta n^*}{\delta M_b^*} = \frac{\frac{1}{2-b} \cdot (\tau_1 \cdot s + 1)}{\tau_1 \cdot \tau_2 \cdot s^2 + (\tau_1 + \tau_2) \cdot s + 1 + \frac{b}{2-b} \cdot \frac{2-a}{e-a}} \quad (15)$$

$$\frac{\delta n^*}{\delta \alpha^*} = \frac{\frac{b}{2-b} \cdot \frac{1}{e-a}}{\tau_1 \cdot \tau_2 \cdot s^2 + (\tau_1 + \tau_2) \cdot s + 1 + \frac{b}{2-b} \cdot \frac{2-a}{e-a}} \quad (16)$$

$$\frac{\delta n^*}{\delta w^*} = \frac{\frac{b}{2-b} \cdot (\tau_1 \cdot s + \frac{e}{e-a})}{\tau_1 \cdot \tau_2 \cdot s^2 + (\tau_1 + \tau_2) \cdot s + 1 + \frac{b}{2-b} \cdot \frac{2-a}{e-a}} \quad (17)$$

$$\frac{\delta n^*}{\delta \theta^*} = -\frac{\frac{q}{2-b} \cdot \left(\tau_1 \cdot s + 1 + \frac{b}{q} \cdot \frac{p}{e-a}\right)}{\tau_1 \cdot \tau_2 \cdot s^2 + (\tau_1 + \tau_2) \cdot s + 1 + \frac{b}{2-b} \cdot \frac{2-a}{e-a}} \quad (18)$$

Likewise the transfer functions from the inputs to the state variable δv_s^* are given by:

$$\frac{\delta v_s^*}{\delta M_b^*} = \frac{\frac{1}{2-b} \cdot \frac{2-a}{e-a}}{\tau_1 \cdot \tau_2 \cdot s^2 + (\tau_1 + \tau_2) \cdot s + 1 + \frac{b}{2-b} \cdot \frac{2-a}{e-a}} \quad (19)$$

$$\frac{\delta v_s^*}{\delta \alpha^*} = -\frac{\frac{1}{e-a} \cdot (\tau_2 \cdot s + 1)}{\tau_1 \cdot \tau_2 \cdot s^2 + (\tau_1 + \tau_2) \cdot s + 1 + \frac{b}{2-b} \cdot \frac{2-a}{e-a}} \quad (20)$$

$$\frac{\delta v_s^*}{\delta w^*} = -\frac{\frac{a}{e-a} \cdot \left(\tau_2 \cdot s + 1 - \frac{b}{2-b} \cdot \frac{2-a}{a}\right)}{\tau_1 \cdot \tau_2 \cdot s^2 + (\tau_1 + \tau_2) \cdot s + 1 + \frac{b}{2-b} \cdot \frac{2-a}{e-a}} \quad (21)$$

$$\frac{\delta v_s^*}{\delta \theta^*} = \frac{\frac{p}{e-a} \cdot \left(\tau_2 \cdot s + 1 - \frac{q}{2-b} \cdot \frac{2-a}{p}\right)}{\tau_1 \cdot \tau_2 \cdot s^2 + (\tau_1 + \tau_2) \cdot s + 1 + \frac{b}{2-b} \cdot \frac{2-a}{e-a}} \quad (22)$$

Note that in these 8 transfer functions, 2 additional parameters are introduced. The first is the effective time constant of the shaft speed loop:

$$\tau_2 \equiv \frac{\tau_n}{2-b} \quad (23)$$

The second parameter is the effective time constant of the ship speed loop:

$$\tau_1 \equiv \frac{\tau_v}{e-a} \quad (24)$$

4.1. Poles, DC-gains and zeros

Analytical derivation of the poles of the transfer functions helps to understand the conditions under which the system is stable or unstable. The derivation of these poles is given in Appendix E. Under the assumptions mentioned there, the first pole can be approximated by:

$$s_1 \cong -\frac{2-bf}{2-b} \cdot \frac{1}{\tau_1} \quad (25)$$

in which f is defined as:

$$f \equiv \frac{e-2}{e-a} \tag{26}$$

Note that for a square resistance law $e = 2 \Rightarrow f = 0$. The second pole can be approximated by:

$$s_2 \cong -\frac{1}{\tau_2} \tag{27}$$

This shows that, under normal conditions where $\tau_2 << \tau_1$, the first pole (in absolute sense) is smaller than the inverse of the ship speed time constant while the second pole corresponds to the inverse of the shaft speed time constant. In normal conditions both poles of the system lie in the left-hand half plane and the core propulsion system is a stable system. The conditions under which the core propulsion system becomes locally unstable can however be derived by determining the circumstances under which the poles of the system (or at least one of the two) lie in the right-hand half plane. This analysis is carried out further on in this paper.

An analytic derivation of all zeros and zero frequency (DC) gains (indicating the gain as ω approaches 0 rad/s) of the 8 transfer functions would lead too far for this paper. An overview of the results of a complete analysis is however given in Table 1. Closer inspection shows that for reasonable values of a, b, p and q, the zero related to the transfer function $\frac{\delta v_s^*}{\delta \theta^*}$ can lie in the right hand half plane, which indicates a non-minimum phase system. In the follow up paper it is shown that the non-minimum phase behaviour quickly disappears after extension of the linearised model with a diesel engine.

The DC-gains of the transfer functions are relevant since they are the sensitivity of the system states to steady state variations in the four inputs. Note that these gains simplify significantly for quadratic resistance curves, where $e = 2$ and as a result $f = 0$.

5. Core system frequency domain behaviour

To get a feeling for the relevance of the transfer functions of the core propulsion system, as given by Eqs. (15) to (22), they are implemented in MATLAB. Realistic values of the parameters a, b, p, q, e, τ_n and τ_v have been determined for a frigate at low cruising speed and are given in Table 2, which also includes some other (derived) parameters which are used in the derivation of the Laplace transfer functions.

The eight Bode plots related to the two system states δn^* and δv_s^* of the core system are shown in Fig. 9, where the response of shaft speed is shown in the left column and the response of ship speed is shown in the right column. An example of how to interpret the Bode plots is given here: The gain of the Bode plot $\frac{\delta n^*}{\delta w^*}$ of the core system is 0.60 at a frequency of 0.1 rad/s, with a phase of -185 degrees (Fig. 9g). This means that at that particular frequency a sinusoidal wake variation of 10% results in a sinusoidal variation of shaft speed of 6%, with a phase lag of 185 degrees. The resulting ship speed variation is much smaller: only 0.9% with a phase lag of 38 degrees. With this interpretation in mind some general observations can be made about these Bode plots:

For the response of shaft and ship speed to engine torque (Figs. 9a and 9b) and resistance variations (Figs. 9e and 9f) the gain falls off gradually with the exception of shaft speed responding to engine torque which remains high until 1 rad/s and only then falls. This behaviour is caused by a zero lying in the neighbourhood of the low frequency pole which forces the amplitude ratio to remain high until the high frequency pole is passed.

The response of shaft speed to wake speed variations (Fig. 9g) also remains quite straight, up to a frequency of 1 rad/s. Its zero almost completely corresponds to the lowest pole frequency. As a result, for wake speed variations the system almost completely behaves as a first order system with a time constant corresponding to the high frequency pole.

The response of ship speed to wake variations (Fig. 9h) is smaller to begin with and falls off much faster, although it also is held back somewhat by a zero lying between the two poles.

The response of shaft speed to pitch variations (Fig. 9c) is very sensitive up to a frequency of 0.5 rad/s, again because its zero is located very close to the lowest pole. After this the transfer function drops of steeply again due to the pole related to the shaft speed.

The response of ship speed to pitch (Fig. 9d) is much smaller again, both static and at higher frequencies. The final descent is initially held back again by a zero lying close to the low frequency pole. Around 0.5 rad/s the transfer function drops steeply again.

Note that a comparison of the linear model behaviour and non-linear model behaviour is given in the follow up paper.

6. Stability Analysis

The stability of a linear system depends on the location of the poles in the complex plane. Appendix E shows that the two poles of the core propulsion system are:

$$s_{1,2} = \frac{-(1+\zeta) \pm \sqrt{(1+\zeta)^2 - \frac{2-bf}{2-b} \cdot 4 \cdot \zeta}}{2 \cdot \zeta \cdot \tau_1} \tag{28}$$

where

$$\zeta \equiv \frac{\tau_2}{\tau_1} \tag{29}$$

Normally the two poles both are non-complex, have negative real part and thus the system is stable. In particular cases the poles can however become complex with negative real parts. In the latter case the system is stable but will show a decaying oscillatory behaviour following a step input. In case the poles have positive real parts the linearised system is (locally) unstable. This does however

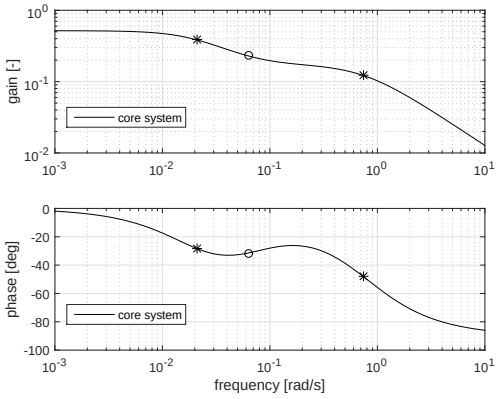

(a) $\frac{\delta n^*}{\delta M_b^*}$.

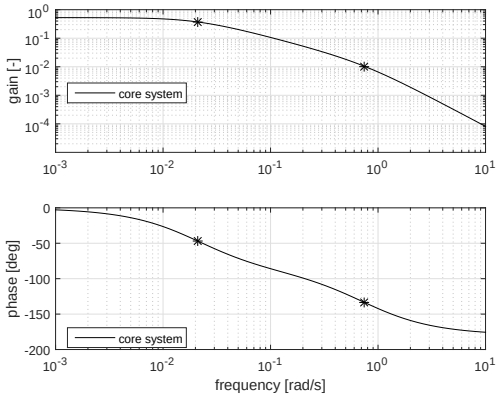

(b) $\frac{\delta v_s^*}{\delta M_b^*}$.

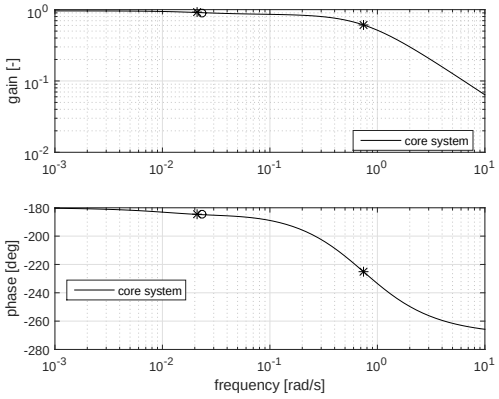

(c) $\frac{\delta n^*}{\delta \theta^*}$.

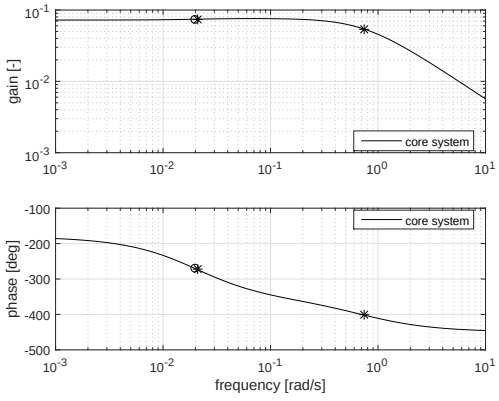

(d) $\frac{\delta v_s^*}{\delta \theta^*}$.

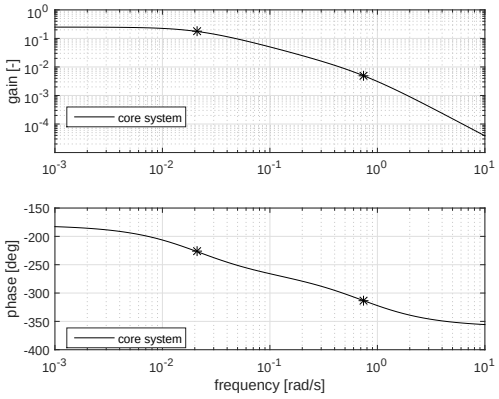

(e) $\frac{\delta n^*}{\delta \alpha^*}$.

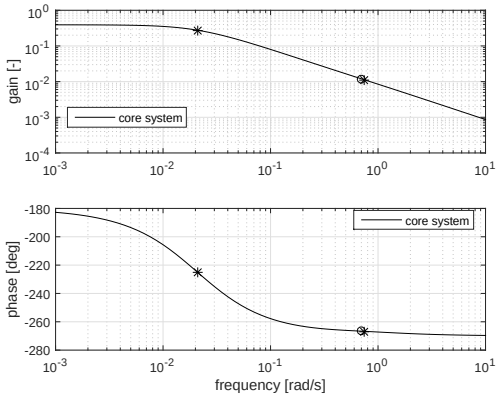

(f) $\frac{\delta v_s^*}{\delta \alpha^*}$.

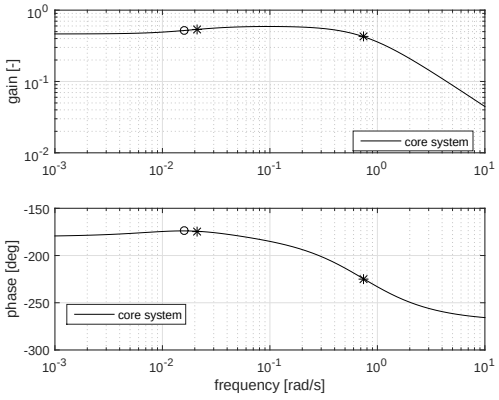

(g) $\frac{\delta n^*}{\delta w^*}$.

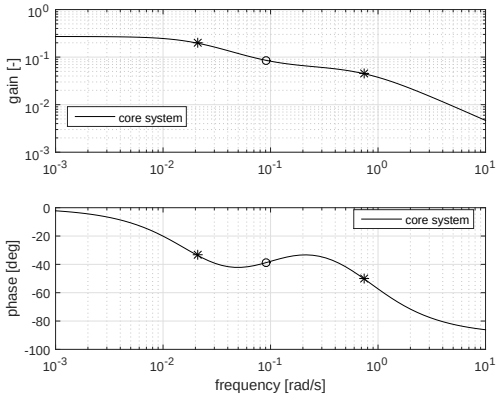

(h) $\frac{\delta v_s^*}{\delta w^*}$.

Figure 9: Open loop Bode plots of shaft speed and ship speed. Poles are indicated by "$*$" and zeros are indicated by "0".

Table 1: Core system zeros, poles and DC-gains.

	Zero $[s^{-1}]$	Pole 1 $[s^{-1}]$	Pole 2 $[s^{-1}]$	DC-gain $G(s)\|_{s=0}$
$\frac{\delta n^*}{\delta M_b^*}$	$-\frac{1}{\tau_1}$	$\approx -\frac{2-bf}{2-b} \cdot \frac{1}{\tau_1}$	$\approx -\frac{1}{\tau_2}$	$\frac{1}{2-bf}$
$\frac{\delta n^*}{\delta \alpha^*}$	none			$\frac{1-f}{2-bf} \cdot \frac{b}{2-a}$
$\frac{\delta n^*}{\delta w^*}$	$-\frac{2-af}{2-a} \cdot \frac{1}{\tau_1}$			$\frac{2-af}{2-bf} \cdot \frac{b}{2-a}$
$\frac{\delta n^*}{\delta \theta^*}$	$-\left(1+\frac{p}{q} \cdot \frac{b(1-f)}{2-a}\right) \cdot \frac{1}{\tau_1}$			$-\frac{1}{2-bf} \cdot \left(q+p \cdot \frac{b(1-f)}{2-a}\right)$
$\frac{\delta v_s^*}{\delta M_b^*}$	none			$\frac{1-f}{2-bf}$
$\frac{\delta v_s^*}{\delta \alpha^*}$	$-\frac{1}{\tau_2}$			$-\frac{1-f}{2-bf} \cdot \frac{2-b}{2-a}$
$\frac{\delta v_s^*}{\delta w^*}$	$-\frac{2}{2-b} \cdot \frac{a-b}{a} \cdot \frac{1}{\tau_2}$			$-\frac{2(1-f)}{2-bf} \cdot \frac{a-b}{2-a}$
$\frac{\delta v_s^*}{\delta \theta^*}$	$-\left(1-\frac{q}{p} \cdot \frac{2-a}{2-b}\right) \cdot \frac{1}{\tau_2}$			$-\frac{1}{2-bf} \cdot \left(q-p \cdot \frac{2-b}{2-a}\right)$

Table 2: Variables and parameters at operating point under consideration.

X_0	16.09	[mm]
$M_{b,0}$	9.10E+04	[Nm]
n_0	1.67	[rps]
J_0	0.93	[-]
F_0	1.90E+05	[N]
$v_{s,0}$	6.83	[m/s]
$K_{T,0}$	0.115	[-]
$K_{Q,0}$	0.0245	[-]
m_{ship}	3211000	[kg]
I_p	68000	$[kgm^2]$
a	-5.4036	[-]
b	-3.499	[-]
p	6.58	[-]
q	5.0245	[-]
e	1.861	[-]
τ_n	7.83	[s]
τ_v	115.69	[s]
τ_1	15.93	[s]
τ_2	1.42	[s]
s_1 approx	-0.0233	$[s^{-1}]$
s_2 approx	-0.7019	$[s^{-1}]$
s_1 exact	-0.0208	$[s^{-1}]$
s_2 exact	-0.7438	$[s^{-1}]$

not automatically mean that the real (non-linear) system is globally unstable. Further analysis of the importance of such a local stability should be supported by a non-linear model, which shows whether and where a new equilibrium exists. From an engineering perspective however local unstable behaviour normally is undesireable, even if the system is globally stable and will find an equilibrium.

The conditions under which the core propulsion system has real or complex poles and is stable or unstable is a multi-dimensional problem due to the 5 variables involved in Eq. (28): a, b, e (because f is a combination of a and e), and τ_v plus τ_n (because these together determine τ_1, τ_2 and ζ). An analysis can be made by setting τ_v and τ_n to realistic values. Subsequently, for a given value of normalised resistance curve steepness e, the pole locations can be calculated in a domain spanned by propeller derivatives a and b. A meaningful visualisation of the results can be given by a complex phase plot which makes use of domain colouring such as given in Fig. 10. The figures present the phase angle of the two poles of the system for 4 different resistance curve steepness values. The normal case where a pole is negative *and* real is indicated by the white area. Left hand plane complex poles are coloured light grey, while right hand plane complex poles are coloured dark grey.

The reasoning behind the selected values of e is as follows: a value of $e = 4$ (the two top figures) indicates a very steep resistance curve while a value of $e = 2$ indicates a quadratic resistance curve. The range between these two values is very typical for a large speed range of displacement ships. A value of $e = 0$ reflects specific parts of the typical resistance curve of planing vessels (see for instance the resistance curve of the double chined planing monohull as studied by van Deyzen (2008). A value of $e = -2$ indicates negative resistance steepness which can only occur locally in the transition from a displacement regime to a planing regime. To have some reference, note that in the example case presented in this paper, $e = 1.86 \approx 2$, and the propeller derivatives are $a = -5.4$ and $b = -3.5$.

Figs. 10a and 10b show that at $e = 4$ (much steeper than

the example case) it is highly unlikely that instability will occur. Even in case the propeller derivatives would for some reason get close to or slightly above zero there is sufficient margin with respect to the dark grey or even medium grey area.

Figs. 10c and 10d show a similar situation at $e = 2$, although in this case the region of instability is increased due to the first pole. It is however unlikely that, even under extreme cavitating conditions resulting in both torque and thrust breakdown leading to positive a and positive b, the operating point will come into the unstable region $a > 2$.

Figs. 10e and 10f show the situation at $e = 0$, where the region of instability has increased even more due to pole 1. Instability could perhaps occur in case the propeller thrust derivative a becomes less negative (due to for instance cavitation), while at the same time the propeller torque derivative b undergoes little change. Whether this is physically possible is questionable because it is expected that torque and thrust breakdown go hand in hand, which is confirmed by the open water diagrams including cavitation as published by Kuiper (1992).

Figs. 10g and 10h show that the stable region becomes small, which is in line with what one would expect at $e = -2$. However, in the real non-linear world such a negative ship resistance steepness would only result in a local temporary unstable condition, and with increase of ship speed following the drop in resistance, a stable region with positive e will be found again. An example of local instability related to a local negative steepness e of the ship resistance curve is investigated by Figari and Altosole (2007).

As was shown here, the stability of the core propulsion system in a specific operating point depends on the normalised propeller derivatives a and b, the normalised resistance curve steepness e and τ_n and τ_v. For normal ships and propulsion systems occurrence of instability is unlikely, especially because similar results were found for other combinations of realistic values of τ_n and τ_v. An instability that could occur is related to a negative or zero resistance curve steepness, even though such a situation is only very local. One could for instance think of hydrofoils or other vessels with very pronounced resistance humps. Other potentially (locally) unstable propulsion systems might include propulsors such as supercavitating or surface piercing propellers of which the open water diagrams can show positive propeller derivatives at low advance ratios.

Although the above discussion on system stability is highly academic, the linearised theory could help to identify potential local instabilities of nonconventional ships or systems. It should however be noted that the stability analysis as carried out here only includes the core propulsion system, without actuators and control system. In future work the stability analysis could be extended to controlled propulsion systems. It should also be noted that the linearised system only helps to identify potential stability issues but to investigate the potential consequences for ship operation a non-linear model is to be used.

7. Conclusions and Recommendations

In this paper a linearised model of the core ship propulsion system was derived in a transparent step by step manner, leading to Bode plots of the system. Verification of the linearised model by comparing its output with the output from a non-linear model is not reported here, but is included in a follow up paper. Furthermore, an analysis of the stability of the core system was carried out, revealing the regions where stability issues might occur. In case a local stability issue is indicated by the linear model it is advised to use a non-linear model to investigate its consequence.

The model derived in this paper provides a solid framework for further work aiming at understanding and improving dynamic behaviour of ship propulsion plants, especially sailing in waves. The linearised model can also be used to determine initial settings of controller parameters, which can subsequently be tested in a non-linear model. There are a multitude of refinements, variations and extensions that can be made to the linearised model:

In this paper the core system is modelled, which means that the static and dynamic characteristics of the relevant actuators (the prime mover and the CPP actuation mechanism) are not included. It is therefore recommended to at least add a prime mover to the core model. The required richness of such a prime mover sub-model depends on the goal that one has with the overall model. For specific cases a static fuel rack map might be sufficient, although a diesel engine model could also be enriched by for instance including dynamics of the turbocharger if interest goes out to other diesel related variables besides engine torque. Furthermore a completely different type of prime mover (such as an electric motor or gas turbine) could be selected and modelled. Extension of the current core model with a CPP hydraulic system is required for model based development of more intelligent multi-variable controllers.

With respect to the propeller the assumption is made that it is a "static" element which does not add dynamics to the system. This in fact is not true for high frequency wakefield variations. To improve understanding of unsteady propeller dynamics and to investigate whether this dynamic effect is important for normal operations it is recommended to develop and implement a dynamic propeller model into the core linearised model. Another recommendation is to model and include a ducted propeller and a water jet into the model. Earlier work related to time domain modelling of dynamic performance performance is reported by Healey et al. (1995), Bachmayer et al. (2000), Blanke et al. (2000) and Pivano et al. (2006). Non-linear time domain modelling of water jets is reported by Altosole et al. (2012) and Campora et al. (2011).

The work regarding the stability analysis of the core system can be extended by considering the stability of a con-

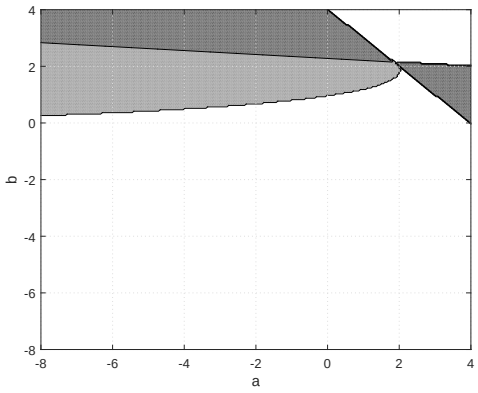

(a) s_1 at $e = 4$

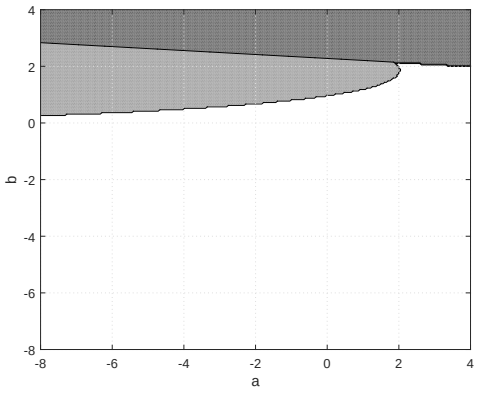

(b) s_2 at $e = 4$

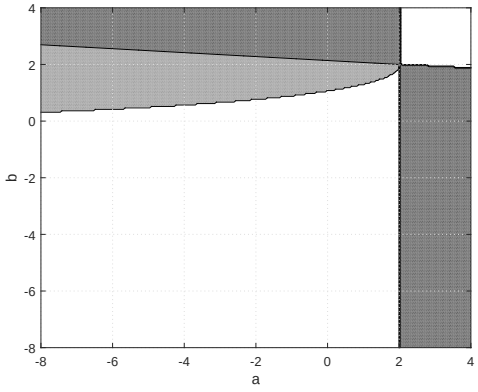

(c) s_1 at $e = 2$

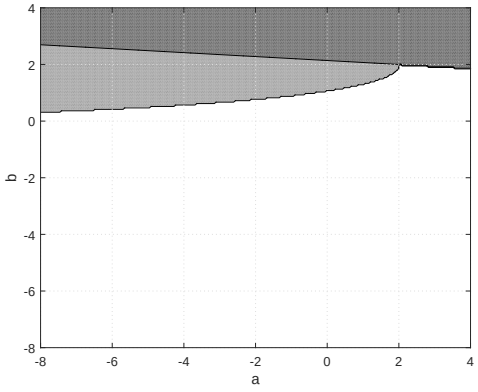

(d) s_2 at $e = 2$

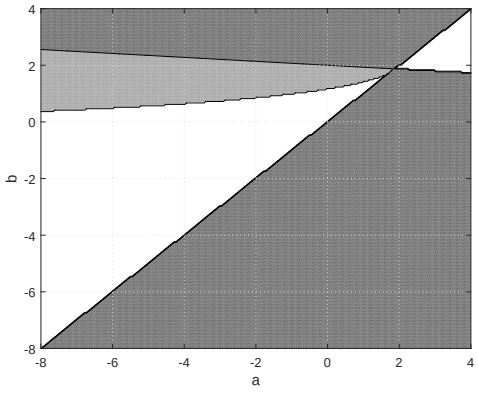

(e) s_1 at $e = 0$

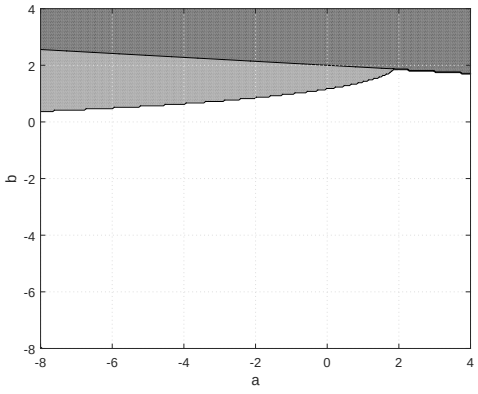

(f) s_2 at $e = 0$

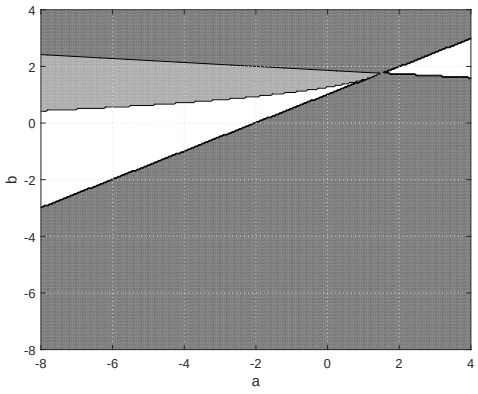

(g) s_1 at $e = -2$

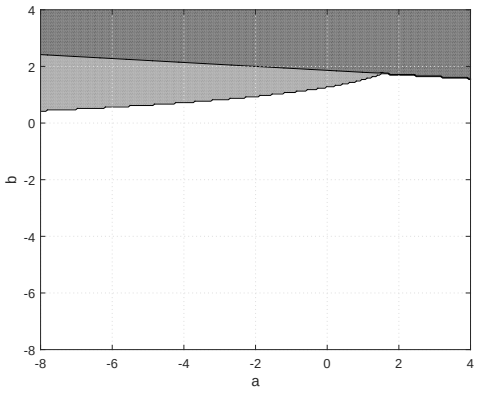

(h) s_2 at $e = -2$

Figure 10: Complex phase plot with domain colouring, $\tau_n = 8s$, $\tau_v = 115s$. The most dark area indicates instability (right hand plane complex poles). The medium grey colour indicates damped oscillatory behaviour (left hand plane complex poles). The white area indicates left hand plane poles without imaginary part.

trolled propulsion system including actuators such that the effect of controller gain settings on stability margins can be made explicit. Another aspect that can be taken up is the systematic gathering and analysis of τ_v and τ_n for a variety of ship types. A collection of their values and ratio could perhaps give valuable insight into the differences and similarities between the behaviour of the propulsion plants of for instance fast and slender lightweight ships compared to slower full-bodied ships.
Besides all aforementioned aspects it is strongly recommended to strengthen future development by, in parallel to the theoretical path, pursuing both a model-scale verification *and* a full-scale validation path.

8. Acknowledgements

The authors are indebted to Albert Wesselink of Wärtsilä Propulsion who came up with the idea to linearise the ship propulsion system during the DYLOPROPS project and pushed Fokke Jan Botke during his MSc thesis work to make the first steps.

References

Altosole, M., Benvenuto, G., Figari, M., Campora, U., 2012. Dimensionless numerical approaches for the performance prediction of marine waterjet propulsion units. Int. J. of Rotating Machinery 2012.

Bachmayer, R., Whitcomb, L., Grosenbaugh, M., Jan 2000. An accurate four-quadrant nonlinear dynamical model for marine thrusters: theory and experimental validation. J. of Ocean. Eng. 25 (1), 146–159.

Blanke, M., 1981. Ship propulsion losses related to automatic steering and prime mover control. Phd thesis, Servolaboratory, Technical University of Denmark, isbn 9788787950145.

Blanke, M., Lindegaard, K., Fossen, T., 2000. Dynamic model for thrust generation of marine propellers. In: 5th IFAC Conf. of Manoeuvring and Control of Marine Craft. pp. 363–368.

Campora, U., Figari, M., Martelli, M., Vignolo, S., Viviani, M., Ratto, M., May 2011. Propulsion plant simulation for fast military vessels. In: Proc. of the 9th Symposium on High Speed Marine Vehicles (HSMV). Naples.

Clarke, D., 1980. Development of a cost function for autopilot optimisation. In: Proceedings of the symposium on Ship Steering Automatic Control. Genova, pp. 59–77.

Dorf, Bishop, 2001. Modern Control Systems, 9th Edition. Prentice Hall.

Figari, M., Altosole, M., Dec. 2007. Dynamic behaviour and stability of marine propulsion systems. Proc. of the Inst. of Mech. Eng., Part M: J. of Eng. for the Marit. Environ. 221 (4), 187–205.

Fossen, T., 1994. Guidance and Control of Ocean Vehicles. John Wiley & Sons, isbn 0471941131.

Franklin, G. F., Powell, J. D., Emami-Naeini, A., 1986. Feedback control of dynamic systems. Vol. 5. Addison-Wesley Reading, MA.

Healey, A. J., Rock, S., Cody, S., Miles, D., Brown, J., Oct. 1995. Towards an improved understanding of thruster dynamics for underwater vehicles. J. of Ocean. Eng. 20 (4), 354–361.

Kidd, P., Munro, N., Thiruarooran, C., Winterborne, D., Feb. 1985. Linear modelling of ship propulsion plants. Proc. Instn. Mech. Engrs. 199 (A1), 53–58.

Kuiper, G., May 1992. The Wageningen Propeller Series. MARIN, marin publication 92-001. Published on the occasion of its 60th anniversary.

Pivano, L., Fossen, T. I., Johansen, T. A., 2006. Nonlinear model identification of a marine propeller over four-quadrant operations. In: the 14th IFAC Symp. Syst. Identification (SYSID).

Shi, W., Mar. 2013. Dynamics of energy system behaviour and emissions of trailing suction hopper dredgers. Phd thesis, Delft University of Technology, isbn 97890-6562-315-7.

Stapersma, D., June 19-23 2000. Interaction between propulsor and engine. In: de Heer, P. (Ed.), Proceedings of the 34th WEGEMT School. Delft University of Technology, Delft, pp. 1–47.

Stapersma, D., Jan. 2016. The general propulsion system block diagram. its linear approximation and associated transfer functions. Internal Report PFS-2003-164, issue D, Delft University of Technology.

van Deyzen, A., Sep. 2008. A nonlinear mathematical model of motions of a planing monohull in head seas. In: Proceedings of the 6th International Conference on High Performance Marine Vehicles. pp. 187–199.

van Spronsen, P. J., Tousain, R., Sep. 2001. An optimal control approach to preventing marine diesel engine overloading aboard Karel Doorman Class frigates. Control Applications in Marine Systems. Delft University Press, pp. 23–30.

van Terwisga, T. J. C., Noble, D. J., van 't Veer, R., Assenberg, F., McNeice, B., van Terwisga, P. F., August 8-13 2004. Effect of operational conditions on the cavitation inception speed of naval propellers. In: Proceedings of the 25th Symposium on Naval Hydrodynamics. Office of Naval Research, National Academies Pres, St. John's, Newfoundland and Labrador.

Xiros, N., 2004. Pid marine engine speed regulation under full load conditions for sensitivity h_∞-norm specification against propeller disturbance. Journal of Marine Engineering and Technology (A5), 3–11.

Appendix A. Nomenclature

Appendix A.1. Notation

a	normalised propeller derivative	[-]
b	normalised propeller derivative	[-]
c	constant	
D	propeller diameter	[m]
e	general exponent	
e	normalised resistance steepness	[-]
F	force	[N]
f	coefficient	[-]
I	moment of inertia	$[kgm^2]$
i	gearbox ratio	[-]
J	advance ratio	[-]
M	torque	[Nm]
m	mass	[kg]
n	rotation speed	[[rps]
P	propeller pitch	[m]
p	normalised propeller derivative	[-]
Q	torque	[Nm]
q	normalised propeller derivative	[-]
R	resistance	[N]
t	time	[s]
t	thrust deduction factor	[-]
v	speed	[m/s]
w	wake fraction	[-]

α	resistance factor	[-]
β	hydrodynamic inflow angle	

ζ	ratio of time constants	[-]
η	efficiency	[-]
θ	propeller pitch angle	[deg]
ρ	density	$[kg/m^3]$
τ	time constant	[s]
τ	integration constant	[s]
ω	frequency	[rad/s]

Appendix A.1.1. Subscripts

0	nominal
a	advance
b	brake
n	shaft speed loop
p	polar
$prop$	propeller
Q	torque
R	relative rotative
r	resultant
s	ship
s	shaft
T	thrust
t	tangential
trm	transmission
v	ship speed loop

Appendix B. Normalisation and Linearisation

Assume a variable that is the product of powers of other variables:

$$Z = c \cdot Y^e \cdot X \tag{B.1}$$

where c is a constant multiplier and e is a constant exponent. In an equilibrium point the variable Z equals:

$$Z_0 = c \cdot Y_0^e \cdot X_0 \tag{B.2}$$

Normalisation of Eq. (B.1) by Eq. (B.2) results in:

$$\frac{Z}{Z_0} = \left(\frac{Y}{Y_0}\right)^e \cdot \frac{X}{X_0} \tag{B.3}$$

If, by definition,

$$X^* \equiv \frac{X}{X_0}, Y^* \equiv \frac{Y}{Y_0}, Z^* \equiv \frac{Z}{Z_0} \tag{B.4}$$

then:

$$Z^* = Y^{*e} \cdot X^* \tag{B.5}$$

Now that the constant value c has been removed by the normalisation, the next step is to remove the non-linearity from Eq. (B.5). Differentiation of Eq. (B.3) by using the chain rule gives:

$$\frac{dZ}{Z_0} = \left(\frac{Y}{Y_0}\right)^e \cdot \frac{dX}{X_0} + e \cdot \left(\frac{Y}{Y_0}\right)^{e-1} \cdot \frac{X}{X_0} \cdot \frac{dY}{Y_0} \tag{B.6}$$

Near equilibrium dX, dY and dZ become small increments δX, δY and δZ. Division of $X = X_0 + \delta X$ by X_0 delivers $\frac{X}{X_0} = 1 + \frac{\delta X}{X_0}$ and likewise $\frac{Y}{Y_0} = 1 + \frac{\delta Y}{Y_0}$. Substitution of this in Eq. (B.6) gives:

$$\frac{\delta Z}{Z_0} = \left(1 + \frac{\delta Y}{Y_0}\right)^e \cdot \frac{\delta X}{X_0} + e \cdot \left(1 + \frac{\delta Y}{Y_0}\right)^{e-1} \cdot \left(1 + \frac{\delta X}{X_0}\right) \cdot \frac{\delta Y}{Y_0} \tag{B.7}$$

Taylor series expansion of Eq. (B.7) and neglecting the second- and higher order terms leaves:

$$\frac{\delta Z}{Z_0} = \frac{\delta X}{X_0} + e \cdot \frac{\delta Y}{Y_0} \tag{B.8}$$

which by introduction of the shorthand notation for differential increment

$$\delta Z^* \equiv \frac{\delta Z}{Z_0} \equiv \frac{Z}{Z_0} - 1 \tag{B.9}$$

this can be written as:

$$\delta Z^* = \delta X^* + e \cdot \delta Y^* \tag{B.10}$$

The latter equation relates the relative change in output Z to the relative change in inputs X and Y, where the constant e, which was present as an exponent in the original Eq. (4) has changed to a constant multiplication factor. Secondly the multiplication of X and Y has turned into a summation. For further background on the linearisation process reference is made to Dorf and Bishop (2001) and Franklin et al. (1986).

The demonstrated concepts of normalisation and linearisation are the basis for the following section where they will be applied to the shaft and ship speed loop of the general ship propulsion block diagram.

Appendix C. Linearisation of shaft speed and ship speed loop

Appendix C.1. The shaft speed loop

The shaft speed dynamics are described by:

$$2\pi \cdot I_p \cdot \frac{dn}{dt} = M_s - M_{prop} \tag{C.1}$$

in which shaft inertia is assumed constant implying that change of mass of water, entrained by the propeller, is neglected. Both shaft and propeller torque vary around equilibrium:

$$M_s = M_{s,0} + \delta M_s \tag{C.2}$$

$$M_{prop} = M_{prop,0} + \delta M_{prop} \tag{C.3}$$

In a steady nominal condition the shaft and propeller torque are equal. In that case:

$$M_{s,0} = M_{prop,0} \tag{C.4}$$

and only the small increments are of importance. This is shown by substitution into Eq. (C.1) and division by nominal torque:

$$\frac{2\pi \cdot I_p}{M_{s,0}} \cdot \frac{n_0}{n_0} \cdot \frac{dn}{dt} = \frac{\delta M_s}{M_{s,0}} - \frac{\delta M_{prop}}{M_{prop,0}} \tag{C.5}$$

Note that this division is only valid for a nominal point that is in equilibrium. Defining the integration constant of the shaft system as:

$$\tau_n \equiv \frac{2\pi \cdot I_p \cdot n_0}{M_{s,0}} \tag{C.6}$$

and defining the normalised shaft speed time-derivative as:

$$\frac{1}{n_0} \cdot \frac{dn}{dt} \equiv \frac{dn^*}{dt} \tag{C.7}$$

delivers:

$$\tau_n \cdot \frac{dn^*}{dt} = \delta M_s^* - \delta M_{prop}^* \tag{C.8}$$

The variables at the right-hand side require further elaboration. The brake engine torque M_b is related to M_s via the gearbox reduction i and the transmission efficiency η_{trm}:

$$M_s = i \cdot \eta_{trm} \cdot M_b \tag{C.9}$$

Normalizing and assumption of constant transmission efficiency gives:

$$\delta M_s^* = \delta M_b^* \tag{C.10}$$

Neglecting the change of relative rotative efficiency, the propeller torque M_{prop}^* equals Q^*:

$$\delta M_{prop}^* = \delta Q^* \tag{C.11}$$

Open water torque Q is related to shaft speed n via the torque coefficient K_Q which comes from the open water diagram: $Q = \rho \cdot n^2 \cdot D^5 \cdot K_Q$. Following the mathematical basis from the previous section this reduces to the following linear equation:

$$\delta Q^* = 2 \cdot \delta n^* + \delta K_Q^* \tag{C.12}$$

K_Q is a function of both the advance coefficient J and the propeller pitch θ: $K_Q = f(J, \theta)$. This relation can be expressed as:

$$\frac{\delta K_Q}{K_{Q,0}} = b \cdot \frac{\delta J}{J_0} + q \cdot \frac{\delta \theta}{\theta_0} \tag{C.13}$$

with the normalised propeller derivatives b and q defined as:

$$b \equiv \frac{J_0}{K_{Q,0}} \cdot \left.\frac{\delta K_Q}{\delta J}\right|_\theta, \quad q \equiv \frac{\theta_0}{K_{Q,0}} \cdot \left.\frac{\delta K_Q}{\delta \theta}\right|_J \tag{C.14}$$

which can be determined using the open water diagram and normalising with equilibrium conditions. Asterisk notation gives:

$$\delta K_Q^* = b \cdot \delta J^* + q \cdot \delta \theta^* \tag{C.15}$$

The normalisation and linearisation of advance ratio J, advance velocity v_a and wake fraction w is not fully written out here, but given as:

$$J = \frac{v_a}{n \cdot D} \Rightarrow \delta J^* = \delta v_a^* - \delta n^* \tag{C.16}$$

$$v_a = (1-w) \cdot v_s \Rightarrow \frac{\delta v_a}{v_{a,0}} = \frac{\delta v_s}{v_{s,0}} - \frac{\delta w}{1-w_0} \Rightarrow$$
$$\delta v_a^* = \delta v_s^* - \delta w^* \tag{C.17}$$

Note that contrary to the transmission losses and the relative rotative efficiency the change of wakefraction is taken into account:

$$\delta w^* = \frac{\delta w}{1-w_0} \tag{C.18}$$

The mathematical description of the shaft speed loop can be written down in short by substitution of Eqs. (C.10), (C.11), (C.12), (C.15), (C.16) and (C.17) into Eq. (C.8). The result gives the relation between shaft acceleration, the two state variables δn^* and δv_s^* and the inputs δM_b^*, δw^* and $\delta \theta^*$:

$$\tau_n \frac{dn^*}{dt} = \delta M_b^* - (2-b)\delta n^* - b\delta v_s^* + b\delta w^* - q\delta\theta^* \tag{C.19}$$

Appendix C.2. The ship speed loop

The dynamics of translational speed of the ship as a differential equation is given by:

$$m_{ship} \cdot \frac{dv_s}{dt} = F_{prop} - F_{ship} \tag{C.20}$$

Note that the ship mass is assumed constant, implying that the change of mass of water, entrained by the hull, is assumed constant.
In the nominal condition:

$$F_{prop} = F_{prop,0} + \delta F_{prop} \tag{C.21}$$

$$F_{ship} = F_{ship,0} + \delta F_{ship} \tag{C.22}$$

assuming equilibrium:

$$F_{prop,0} = F_{ship,0} \tag{C.23}$$

so that:

$$m_{ship} \cdot \frac{dv_s}{dt} = \delta F_{prop} - \delta F_{ship} \tag{C.24}$$

Division by the nominal force and introducing the integrator constant of ship translation:

$$\tau_v \equiv \frac{m_{ship} \cdot v_{s,0}}{F_{ship,0}} \tag{C.25}$$

and

$$\frac{1}{v_{s,0}} \cdot \frac{dv_s}{dt} \equiv \frac{dv_s^*}{dt} \tag{C.26}$$

gives

$$\tau_v \cdot \frac{dv_s^*}{dt} = \delta F_{prop}^* - \delta F_{ship}^* \tag{C.27}$$

The forces on the right- hand side now require elaboration. The ship force F_{ship} is replaced by the resistance force R:

$$\frac{\delta F_{ship}}{F_{ship,0}} = \frac{\delta R}{R_0} \Rightarrow \delta F^*_{ship} = \delta R^* \tag{C.28}$$

Note that this replacement is carried out to allow for inclusion of additional forces at a later stage, such as for instance due to a fishing net or dredging suction head dragging over the bottom. Assume the resistance curve as:

$$R = \alpha \cdot v_s^e \Rightarrow \frac{\delta R}{R_0} = \frac{\delta \alpha}{\alpha_0} + e \cdot \frac{\delta v_s}{v_{s,0}} \tag{C.29}$$

In asterisk notation this gives:

$$\delta R^* = \delta \alpha^* + e \cdot \delta v_s^* \tag{C.30}$$

Obviously the normalised steepness e of the resistance curve is formally defined as:

$$e \equiv \frac{v_{s,0}}{R_0} \cdot \frac{\delta R}{\delta v_s}\bigg|_{\alpha} \tag{C.31}$$

The force delivered by the number of propellers "k_p" is a result of the open water thrust T and the thrust deduction factor t:

$$F_{prop} = k_p \cdot (1-t) \cdot T \Rightarrow \frac{\delta F_{prop}}{F_{prop,0}} = \frac{\delta T}{T_0} - \frac{\delta t}{1-t_0} \tag{C.32}$$

If the thrust deduction factor is assumed constant, then:

$$\delta F^*_{prop} = \delta T^* \tag{C.33}$$

The open water thrust T is obtained by:

$$T = \rho \cdot n^2 \cdot D^4 \cdot K_T \Rightarrow \frac{\delta T}{T_0} = 2 \cdot \frac{\delta n}{n_0} + \frac{\delta K_T}{K_{T,0}} \Rightarrow \delta T^* = 2 \cdot \delta n^* + \delta K^*_T \tag{C.34}$$

The thrust coefficient is treated in the same way as the torque coefficient: K_T is a function of both the advance ratio J and the propeller pitch: $K_T = g(J, \theta)$. This relation can be expressed as:

$$\frac{\delta K_T}{K_{T,0}} = a \cdot \frac{\delta J}{J_0} + p \cdot \frac{\delta \theta}{\theta_0} \tag{C.35}$$

with the normalised propeller derivatives a and p defined as:

$$a \equiv \frac{J_0}{K_{T,0}} \cdot \frac{\delta K_T}{\delta J}\bigg|_{\theta}, \quad p \equiv \frac{\theta_0}{K_{T,0}} \cdot \frac{\delta K_T}{\delta \theta}\bigg|_{J} \tag{C.36}$$

so that in asterisk notation:

$$\delta K^*_T = a \cdot \delta J^* + p \cdot \delta \theta^* \tag{C.37}$$

The linearised differential equation for the ship speed loop is obtained by substitution of Eqs. (C.16), (C.17), (C.28), (C.30), (C.33), (C.34) and (C.37) into Eq. (C.27). The result gives the relation between ship acceleration, the two system states and $\delta\alpha^*$, δw^* and $\delta\theta^*$.

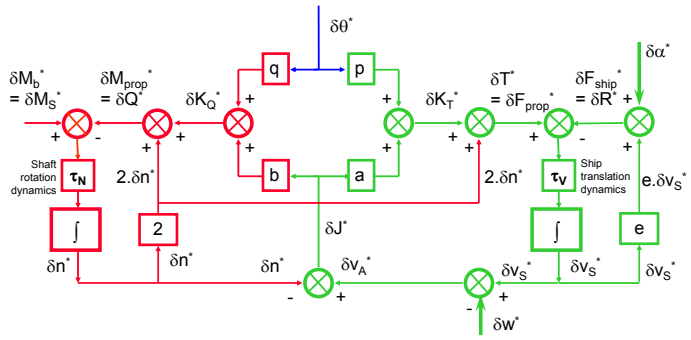

Figure C.11: Vertically oriented linearised block diagram of the core propulsion system.

$$\tau_v \frac{dv_s^*}{dt} = (2-a)\delta n^* - (e-a)\delta v_s^* - \delta\alpha^* - a\delta w^* + p\delta\theta^* \tag{C.38}$$

Concatenation of Eqs. (C.8), (C.10), (C.11), (C.12), (C.15), (C.16), (C.17), (C.27), (C.28), (C.30), (C.33), (C.34) and (C.37) in block diagram form leads to Fig. C.11. Note that many other equivalent block diagrams can be drawn and the version shown here not necessarily has the simplest form. It does however clearly demonstrate the relation with the non-linear block diagram as shown in Fig. 2.

Appendix D. Linearisation of four quadrant propeller performance

Although in the main text only the one quadrant $J - K_T - K_Q$ diagram was considered, a system modelled with a four quadrant $\beta - C_T^* - C_Q^*$ diagram can also be linearised. In the four quadrant framework the inflow angle β is defined as:

$$\beta = \arctan\left(\frac{v_a}{0.7\pi n D}\right) \tag{D.1}$$

By application of the Taylor expansion of $\arctan(x)$ and neglecting higher order terms we get :

$$\beta = \arctan\left(\frac{v_a}{0.7\pi n D}\right) \approx \frac{v_a}{0.7\pi n D} \tag{D.2}$$

Normalisation of the differential increment gives:

$$\delta\beta^* = \delta v_a^* - \delta n^* \tag{D.3}$$

The four quadrant thrust and torque coefficients are defined as:

$$C'_T = \frac{T}{1/2\rho v_r^2 \pi/4D^2} = \frac{T}{\rho v_r^2 \pi/8D^2}$$
$$C'_Q = \frac{Q}{1/2\rho v_r^2 \pi/4D^3} = \frac{Q}{\rho v_r^2 \pi/8D^3} \tag{D.4}$$

Note that by convention the four quadrant thrust and torque coefficients C_T^* and C_Q^* are noted with an asterisk.

In this paper this convention is not kept to avoid using double asterisk notation. Instead the $C_T^{'}$ and $C_Q^{'}$ notation is used to indicate the use of four quadrant coefficients. Further note that v_r is the resultant inflow speed, based on axial inflow v_a and tangential inflow $v_t = 0.7\pi nD$ via:

$$v_r^2 = v_a^2 + v_t^2 \tag{D.5}$$

Therefore

$$(v_{r,0} + \delta v_r)^2 = (v_{a,0} + \delta v_a)^2 + (v_{t,0} + \delta v_t)^2 \tag{D.6}$$

which can be written out as:

$$v_{r,0}^2 + 2v_{r,0}\delta v_r + \delta v_r^2 = \tag{D.7}$$
$$v_{a,0}^2 + 2v_{a,0}\delta v_a + \delta v_a^2 + v_{t,0}^2 + 2v_{t,0}\delta v_t + \delta v_t^2$$

Neglecting higher order terms and simplification gives:

$$v_{r,0}\delta v_r = v_{a,0}\delta v_a + v_{t,0}\delta v_t \tag{D.8}$$

Normalisation with $v_{r,0}^2$ gives

$$\frac{\delta v_r}{v_{r,0}} = \frac{v_{a,0}\delta v_a}{v_{r,0}^2} + \frac{v_{t,0}\delta v_t}{v_{r,0}^2} \tag{D.9}$$

which equals:

$$\frac{\delta v_r}{v_{r,0}} = \left(\frac{v_{a,0}}{v_{r,0}}\right)^2 \frac{\delta v_a}{v_{a,0}} + \left(\frac{v_{t,0}}{v_{r,0}}\right)^2 \frac{\delta v_t}{v_{t,0}} \Rightarrow \tag{D.10}$$
$$\delta v_r^* = z\delta v_a^* + (1-z)\delta v_t^* = z\delta v_a^* + (1-z)\delta n^*$$

in which

$$z = \left(\frac{v_{a,0}}{v_{r,0}}\right)^2 = \sin^2\beta_0 \tag{D.11}$$

Analogue to the derivation of propeller derivatives in the one quadrant open water diagram, the propeller derivatives in the four quadrant diagram are defined as:

$$a' \equiv \frac{\beta_0}{C'_{T,0}} \cdot \frac{\delta C'_T}{\delta\beta},\ p' \equiv \frac{\theta_0}{C'_{T,0}} \cdot \frac{\delta C'_T}{\delta\theta} \tag{D.12}$$
$$b' \equiv \frac{\beta_0}{C'_{Q,0}} \cdot \frac{\delta C'_Q}{\delta\beta},\ q' \equiv \frac{\theta_0}{C'_{Q,0}} \cdot \frac{\delta C'_Q}{\delta\theta}$$

where again the $'$ notation is used to indicate use of the four quadrant diagram. The thrust and torque coefficients are now given by:

$$\delta C_T^{'*} = a' \cdot \delta\beta^* + p' \cdot \delta\theta^* \tag{D.13}$$
$$\delta C_Q^{'*} = b' \cdot \delta\beta^* + q' \cdot \delta\theta^*$$

The thrust and torque are defined by:

$$T = C_T^{'} \cdot \frac{\rho v_r^2 \pi D^2}{8} \tag{D.14}$$
$$Q = C_Q^{'} \cdot \frac{\rho v_r^2 \pi D^3}{8}$$

which in asterisk form gives:

$$\delta T^* = \delta C_T^{'*} + 2\delta v_r^* \tag{D.15}$$
$$\delta Q^* = \delta C_Q^{'*} + 2\delta v_r^*$$

Finally the four quadrant equivalent version of Eqs. (9) and (10) can now be written as:

$$\tau_n \frac{dn^*}{dt} = \delta M_b^* - (2 - b' - 2z)\delta n^* \tag{D.16}$$
$$-(b' + 2z)\delta v_s^* + (b' + 2z)\delta w^* - q'\delta\theta^*$$

$$\tau_v \frac{dv_s^*}{dt} = (2 - a' - 2z)\delta n^* - (e - a' - 2z)\delta v_s^* \tag{D.17}$$
$$-\delta\alpha^* - (a' + 2z)\delta w^* + p'\delta\theta^*$$

Appendix E. Laplace Transfer Functions

The derivation and analysis of the Laplace transfer functions of the core propulsion system based on Stapersma (2016) is presented in this Appendix. Starting with the differential Eq. (C.19) for shaft speed, the Laplace operator is introduced which gives:

$$(\tau_n s + (2 - b))\,\delta n^* = \delta M_b^* - b\delta v_s^* + b\delta w^* - q\delta\theta^* \tag{E.1}$$

which is a first order equation with 4 inputs on the right hand side. Written in canonical form:

$$(\tau_2 s + 1)\,\delta n^* = \tag{E.2}$$
$$\frac{1}{2-b}\delta M_b^* - \frac{b}{2-b}\delta v_s^* + \frac{b}{2-b}\delta w^* - \frac{q}{2-b}\delta\theta^*$$

where the effective time constant of the shaft speed loop is:

$$\tau_2 \equiv \frac{\tau_n}{2-b} \tag{E.3}$$

On the right hand side the ship speed appears, for which another differential equation can be derived analogously. Starting from Eq. (C.38) this gives:

$$(\tau_1 s + 1)\,\delta v_s^* = \tag{E.4}$$
$$\frac{2-a}{e-a}\delta n^* - \frac{1}{e-a}\delta\alpha^* - \frac{a}{e-a}\delta w^* + \frac{p}{e-a}\delta\theta^*$$

where the effective time constant of the ship speed loop is:

$$\tau_1 \equiv \frac{\tau_v}{e-a} \tag{E.5}$$

Substitution of Eq. (E.4) into Eq. (E.2) and grouping together gives:

$$\left(\tau_1\tau_2 s^2 + (\tau_1 + \tau_2)s + 1 + \frac{b}{2-b}\cdot\frac{2-a}{e-a}\right)\delta n^* =$$
$$+\frac{1}{2-b}(\tau_1 s + 1)\,\delta M_b^*$$
$$+\frac{b}{2-b}\cdot\frac{1}{e-a}\delta\alpha^*$$
$$+\frac{b}{2-b}\left(\tau_1 s + 1 + \frac{a}{e-a}\right)\delta w^*$$
$$-\frac{q}{2-b}\left(\tau_1 s + 1 + \frac{b}{q}\cdot\frac{p}{e-a}\right)\delta\theta^* \tag{E.6}$$

which is a second order system with 4 inputs on the right hand side. This results in four transfer functions for shaft speed, which are given in Section 4. The transfer functions for ship speed can be derived by substitution of Eq. (E.2) into (E.4) in order to eliminate shaft speed. Without giving the full derivation this leads to the 4 transfer functions also given in Section 4.
Analytical derivation of the poles of these 8 transfer functions helps to understand the conditions under which the system is stable or unstable. The derivation of these poles starts with the characteristic equation by setting the denominator of the transfer functions to zero:

$$\tau_1\tau_2 s^2 + (\tau_1+\tau_2)s + 1 + \frac{b}{2-b}\cdot\frac{2-a}{e-a} = 0 \qquad \text{(E.7)}$$

Introduce:

$$1 - f \equiv \frac{2-a}{e-a} \qquad \text{(E.8)}$$

or

$$f \equiv \frac{e-2}{e-a} \qquad \text{(E.9)}$$

Note that for a square resistance law $e = 2 \Rightarrow f = 0$. Reshuffle the constant part of the characteristic equation such that:

$$1 + \frac{b}{2-b}(1-f) = \frac{2-bf}{2-b} \qquad \text{(E.10)}$$

Also introduce the ratio of the two effective time constants:

$$\zeta \equiv \frac{\tau_2}{\tau_1} \qquad \text{(E.11)}$$

Normally the shaft speed loop is much faster than the ship speed loop meaning that its time constant is much shorter: $\tau_2 < \tau_1$, in which case $\zeta < 1$. By replacing the effective time constant of the shaft speed loop by its ratio with the ship speed time constant $\tau_2 = \zeta \cdot \tau_1$, the characteristic equation becomes:

$$\zeta\cdot\tau_1^2\cdot s^2 + (1+\zeta)\tau_1 s + \frac{2-bf}{2-b} = 0 \qquad \text{(E.12)}$$

Division by τ_1 gives:

$$\zeta\cdot\tau_1\cdot s^2 + (1+\zeta)s + \frac{2-bf}{2-b}\frac{1}{\tau_1} = 0 \qquad \text{(E.13)}$$

The poles of the characteristic equation are obtained with the ABC formula and are given by:

$$s_{1,2} = \frac{-(1+\zeta) \pm \sqrt{(1+\zeta)^2 - \frac{2-bf}{2-b}\cdot 4\cdot\zeta}}{2\cdot\zeta\cdot\tau_1} \qquad \text{(E.14)}$$

These poles can be calculated directly or can be approximated in case $\tau_2 << \tau_1 \Rightarrow \zeta << 1$. In that case:

$$\begin{aligned} s_{1,2} &= \frac{-(1+\zeta) \pm (1+\zeta)\sqrt{1 - \frac{2-bf}{2-b}\cdot\frac{4\cdot\zeta}{(1+\zeta)^2}}}{2\cdot\zeta\cdot\tau_1} \\ &\cong \frac{-(1+\zeta) \pm (1+\zeta)\left(1 - \frac{1}{2}\frac{2-bf}{2-b}\cdot\frac{4\cdot\zeta}{(1+\zeta)^2}\ldots\right)}{2\cdot\zeta\cdot\tau_1} \\ &\cong \frac{-(1+\zeta) \pm (1+\zeta)\left(1 - \frac{2-bf}{2-b}\cdot 2\cdot\zeta(1-2\zeta\ldots)\ldots\right)}{2\cdot\zeta\cdot\tau_1} \\ &\cong \frac{-(1+\zeta) \pm \left(1+\zeta - \frac{2-bf}{2-b}\cdot 2\cdot\zeta\ldots\right)}{2\cdot\zeta\cdot\tau_1} \end{aligned} \qquad \text{(E.15)}$$

The first pole is approximated by:

$$\begin{aligned} s_1 &\cong \frac{-(1+\zeta) + \left(1+\zeta - \frac{2-bf}{2-b}\cdot 2\cdot\zeta\right)}{2\cdot\zeta\cdot\tau_1} \\ &\cong -\frac{2-bf}{2-b}\cdot\frac{1}{\tau_1} \end{aligned} \qquad \text{(E.16)}$$

and the second pole is approximated by:

$$\begin{aligned} s_2 &\cong \frac{-(1+\zeta) - \left(1+\zeta - \frac{2-bf}{2-b}\cdot 2\cdot\zeta\right)}{2\cdot\zeta\cdot\tau_1} \\ &\cong -\frac{1}{\zeta\cdot\tau_1} + \frac{b(1-f)}{2-b}\cdot\frac{1}{\tau_1} \\ &\cong -\frac{1}{\tau_2} \end{aligned} \qquad \text{(E.17)}$$